Singlet and Triplet Excited-State Dynamics of a Nonfullerene Electron Acceptor Y6

AUTHOR NAMES;

Shin-ichiro Natsuda[1], Yuji Sakamoto[1], Taiki Takeyama[1], Rei Shirouchi[1], Toshiharu Saito[1], *Yasunari Tamai[1,2*], Hideo Ohkita[1]*

AUTHOR ADDRESS;

[1]Department of Polymer Chemistry, Graduate School of Engineering, Kyoto University, Katsura, Nishikyo, Kyoto 615-8510, Japan

[2]Japan Science and Technology Agency (JST), PRESTO, 4-1-8 Honcho Kawaguchi, Saitama 332-0012, Japan

ABSTRACT

Understanding the excited-state dynamics of nonfullerene electron acceptors is essential for further improvement of organic solar cells as they are responsible for near-IR light absorption. Herein, we investigated the singlet and triplet excited-state dynamics in Y6, a novel nonfullerene acceptor, using transient absorption spectroscopy. We found that, even at low excitation fluences, pristine Y6 films show biphasic singlet exciton decay kinetics with decay constants of ~220 ps and ~1200 ps. The majority of the Y6 singlet excitons decayed with the faster (~220 ps) component, whereas a clear photoluminescence with the slower (~1200 ps) component was observed, which is the origin of the large discrepancies in the previously reported exciton lifetimes of Y6 in the solid state. At high excitation fluences, on the other hand, Y6 singlet excitons are more likely to decay via singlet–singlet exciton annihilation due to fast exciton diffusion in crystalline domains, after which we observed ultrafast triplet formation, assigned to singlet fission from higher excited singlet states.

TOC GRAPHICS

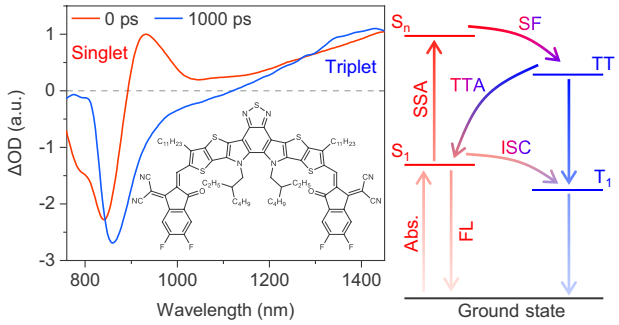

KEYWORDS: exciton diffusion, organic solar cell, photon upconversion, singlet–singlet exciton annihilation, singlet fission, transient absorption spectroscopy

Introduction

The power conversion efficiencies (PCEs) of organic solar cells (OSCs) now exceed 18%,[1-3] largely owing to the development of novel nonfullerene acceptors (NFAs).[4-12] OSCs consisting of a low-bandgap NFA and a wide-bandgap donor polymer exhibit strong and complementary absorption in the visible to near-IR region, resulting in efficient photocurrent generation comparable to their inorganic counterparts. This is in sharp contrast to conventional fullerene-based OSCs, wherein mainly donor polymers are responsible for photon absorption due to the small absorption cross-section of fullerenes in the visible to near-IR regions, thereby singlet excitons are predominantly generated in the donor polymers. Therefore, significant efforts have been made to understand excited-state properties of donor polymers over the past three decades. In contrast, NFAs are responsible for near-IR light absorption for recent NFA-based OSCs. Hence, currently, it has become increasingly important to understand the excited-state dynamics of NFAs. However, compared to donor polymers, relatively little is known about the excited-state dynamics of NFAs.

State-of-the-art OSCs often use Y6 (the chemical structure, steady-state absorption, and photoluminescence (PL) spectra of Y6 are found in Figure S1) and its derivatives as NFAs. These NFAs are strongly crystalline and exhibit deep highest occupied molecular orbital (HOMO) energy levels, large absorption cross-sections in the near-IR region, and optical bandgaps suitable for solar cell applications. Therefore, a lot of studies on Y6-based OSCs have been conducted.[13-19] In contrast, the excited-state properties of Y6 are still not fully understood. For example, the singlet exciton diffusion length L_D, which is defined as $L_D = (D\tau)^{0.5}$, where D is the exciton diffusion constant and τ is the exciton lifetime, is an important parameter that affects the PCE. Nevertheless, the reported τ values for Y6 thin films cover a significant range, from ~50 ps to ~1.8 ns.[20-25]

Therefore, further research is necessary to understand the origins of such large discrepancies as well as reliable excited-state properties. Alongside singlet excited-state properties, those of triplet excited states are also important. In OSCs, bimolecular charge recombination leads to the formation of both singlet and triplet charge transfer (CT) states with a ratio of 1:3. The triplet CT state subsequently decays to a lower-lying triplet excited state on either donor or acceptor material, which then re-dissociates into the CT state or otherwise is quenched by charges or other triplets. As the CT–triplet transition rate depends on the energy difference between these states, the triplet excited state energy of Y6 is important for the charge recombination/re-generation dynamics in OSCs.[26,27]

Herein, we study the singlet and triplet excited-state dynamics of Y6 in the solid state using transient absorption (TA) spectroscopy. We found that pristine Y6 films show biphasic singlet exciton decay kinetics with decay constants of ~220 ps and ~1200 ps, which is the origin of the large discrepancies in the previously reported exciton lifetimes of Y6 in the solid state. Y6 shows a relatively large exciton diffusion constant and a small energy difference between the lowest excited singlet and triplet states (S_1 and T_1 states). Ultrafast triplet exciton formation was observed at high excitation fluences, which is attributable to singlet fission from higher excited singlet states (S_n states) generated through singlet–singlet exciton annihilation (SSA).

Experimental Methods

Film preparation. Films for all spectroscopic measurements were prepared on quartz substrates, which were successively cleaned by sonication in toluene, acetone, and ethanol for 15 min each. Y6 was dissolved in chloroform (CF) and left to stir at room temperature overnight. Thin films were spin-coated onto the cleaned substrates in a N_2-filled glovebox and then thermally annealed

at 110 °C for 5 min. For TA and time-resolved PL (TRPL) measurements, the samples were encapsulated in the glovebox.

Measurements

Steady-state absorption and PL spectra. UV–visible absorption spectra were acquired using a UV–visible spectrometer (Hitachi, U-4100). The PL spectra were measured using a fluorescence spectrophotometer (Horiba Jobin Yvon, NanoLog) equipped with a photomultiplier tube (Hamamatsu, R928P) and a liquid-N_2-cooled InGaAs near-IR array detector (Horiba Jobin Yvon, Symphony II). The excitation wavelength was set to 790 nm. The PL decay kinetics were measured by the time-correlated single-photon-counting (TCSPC) method (Horiba Jobin Yvon, FluoroCube). PL quantum yield (PLQY) was measured using an absolute QY measurement system (Bunko-keiki, BEL-300) with an integrating sphere.

TA measurements. Femtosecond TA data were collected using a pump and probe femtosecond TA spectroscopy system, which consisted of a TA spectrometer (Ultrafast Systems, Helios) and a regenerative amplified Ti:sapphire laser (Spectra-Physics, Hurricane). Basically, the fundamental pulse with a wavelength of 800 nm was used for the excitation source, and when necessary, pump pulses of shorter wavelengths, generated with an ultrafast optical parametric amplifier (Spectra-Physics, TOPAS, for 700 and 530 nm) and a second harmonic generator (Spectra-Physics, TP-F, for 400 nm), were used. The TA data were collected over a time range from −5 ps to 3 ns.

Microsecond TA data were collected using a sensitive microsecond TA system. A Nd:YAG laser (Elforlight, SPOT-10-200-532) operating at a wavelength of 532 nm was used as the excitation source. White light from a tungsten lamp with a stabilized power source was used as the probe

light. Two monochromators and appropriate optical cut-off filters were placed before and after the sample to increase the signal-to-noise ratio (SNR). Further details of our TA setup have been presented elsewhere.[28]

Density functional theory (DFT) calculations. DFT calculations were carried out for the isolated Y6 molecule, where alkyl side chains were shortened to reduce the computational effort, using the Gaussian 16 rev. A package.[29] The Y6 molecule was optimized using the B3LYP functional and 6-311G(d,p) basis set in the ground state, whereas time-dependent (TD)-DFT with B3LYP/6-31+G(d) within the Tamm–Dancoff approximation was performed for the T_1 state optimization.[30] The energy level of the T_1 state E_{T1} was calculated as the average of the two vertical excitation energies at the optimized T_1 and ground-state geometries.

Results and Discussion

Assignment of TA spectra. Figure 1a shows the TA spectra of a pristine Y6 film (70 nm thick). A photoinduced absorption (PIA) band at ~930 nm and a broad tail above 1200 nm appeared immediately after photoexcitation at 800 nm. These bands are assigned to Y6 singlet excitons in the solid state because its spectral shape is similar to the Y6 singlet PIA in a CF solution except the red-shift of the spectrum (Figure S2).[31] In addition, a sharp negative signal was observed at ~850 nm, which is attributable to the ground-state bleaching (GSB) of Y6. Singlet excitons decayed with time. On the nanosecond time scale, the singlet PIA completely disappeared, instead a weak long-lived PIA was observed at 1400 nm. The long-lived PIA was also observed for Y6 in the CF solution, wherein we attribute it to triplet excitons generated through intersystem crossing (ISC) (see Figures S2 and S3). In contrast, the long-lived PIA was not clearly observed for the

pristine Y6 film, most likely due to the lower SNR achieved by keeping the excitation fluence as low as possible to reduce the contribution of SSA. Therefore, we sensitized Y6 using Pt(II)octaethylporphyrin (PtOEP), a well-known triplet sensitizer.[32] Figure 1b shows the TA spectrum of a Y6/PtOEP blend film (7:1 w/w) monitored 1 ns after photoexcitation at 530 nm, which reveals a large PIA band at ~1400 nm similar to that of the Y6 triplet excitons observed in the CF solution. This band was still observed on the microsecond time scale (Figure S4). Thus,

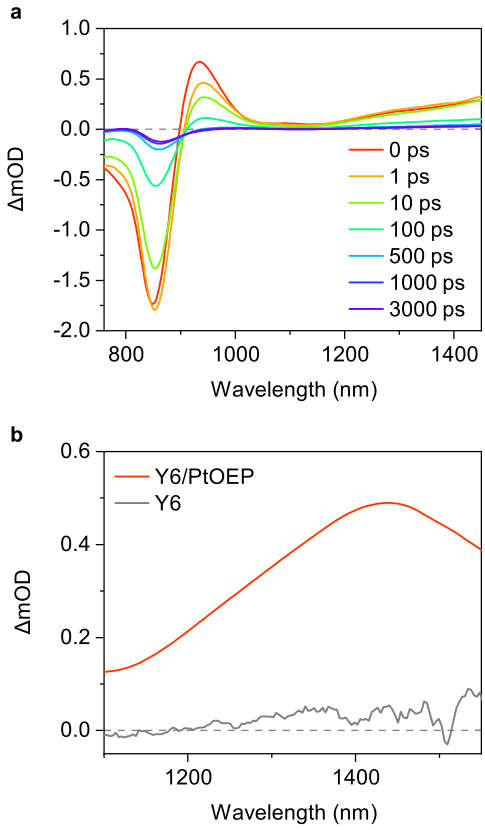

Figure 1. (a) TA spectra of a pristine Y6 film (70 nm thick). The excitation wavelength was set to 800 nm with a fluence of 3.8 μJ cm^{-2}. (b) TA spectra of a Y6/PtOEP blend (7:1 w/w) film and a pristine Y6 film as a reference monitored at 1000 ps after photoexcitation. The excitation wavelength was set to 530 nm, which is the peak wavelength of PtOEP absorption, with a fluence of 5.0 μJ cm^{-2}.

this band is assigned to the T_1–T_n absorption of Y6 in the solid state. To briefly summarize the wavelengths we will be focusing on, Y6 shows the GSB signal at ~850 nm, singlet exciton absorption at ~930 nm and >1200 nm, and triplet exciton absorption at ~1400 nm.

Singlet exciton lifetime. In TA measurements, the bimolecular exciton deactivation process due to SSA generates an additional decay channel that leads to faster exciton decay.[33,34] Hence, SSA must be avoided when the intrinsic singlet exciton decay kinetics is observed. Because it is difficult to avoid SSA in the thin Y6 film, which, as discussed later, is a sign of fast exciton diffusion, we performed TA measurements for a 240 nm thick film (the TA spectra of the thick Y6 film are presented in Figure S5) with weak excitation fluences. The excitation wavelength was set to 400 nm, where the absorption cross-section of Y6 is approximately six times smaller than that at the peak wavelength, to keep the exciton density low. Figure 2a shows the excitation-fluence dependence of the exciton decay kinetics monitored at 930 nm. The decay kinetics are independent of the excitation fluence, at least below 3.0 μJ cm^{-2}; however, decay was slightly faster at 6.4 μJ cm^{-2} owing to SSA. We simultaneously fitted the two fluences (3.0 μJ cm^{-2} and 2.2 μJ cm^{-2}) with a shared time constant. The exciton decay was well fitted by an exponential function with a lifetime of ~220 ps. Note that the decay kinetics of the broad PIA tail above 1200 nm at early times were also well reproduced by the same exponential function, indicating that mainly singlet excitons are responsible for this region at early times.

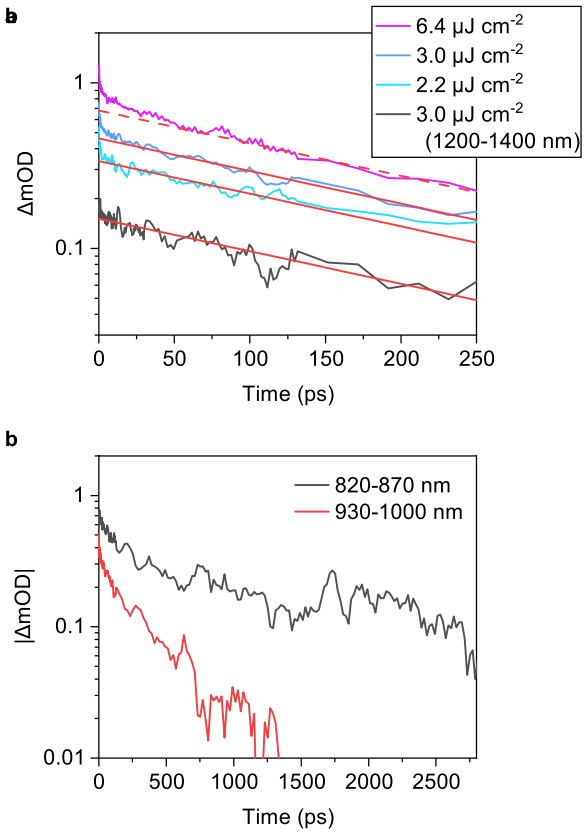

Figure 2. (a) Time evolution of TA signals monitored at 930 nm at various excitation fluences. The excitation wavelength was set to 400 nm. A 240 nm thick pristine Y6 film was used to avoid SSA. The black line represents the decay kinetics of the TA signals averaged over the 1200–1400 nm region. The red lines represent the best fitted exponential curves. (b) Time evolution of TA signals at later times. TA signals were averaged over wide spectral regions as indicated to improve the SNR. The GSB signals were reversed in sign. Time evolution for the 1200–1400 nm region is not shown because the SNR on the nanosecond time scale is too low to be discussed in detail.

Interestingly, the singlet exciton lifetime measured by TA spectroscopy is significantly shorter than the PL decay lifetime obtained by the TCSPC method (~1.2 ns, Figure S6). As mentioned above, this large discrepancy has also been reported previously: exciton lifetimes of a few

hundreds of picoseconds were obtained by TA measurements, whereas lifetimes of >1 ns were obtained by TRPL measurements.[21-25] Close inspection of the TA spectra (Figures 1a and S5) reveals that the TA signal in the 900–950 nm region turned into negative at later times, which is attributable to the stimulated emission (SE) of Y6 because its spectral position coincides with the PL spectrum (Figure S1). This indicates that SE with a longer time constant can also be observed in the TA spectra. Importantly, however, this means that SE was observed despite that the singlet exciton absorption had already disappeared at later times.

At later times, as shown in Figure 2b, singlet excitons (red line) decayed considerably faster than the GSB (black line), indicating that the majority of transient species presented at later times are triplet excitons. Triplet excitons, then, decayed on the nanosecond time scale (Figures 2b and S5), suggesting the presence of triplet–triplet exciton annihilation (TTA) because decay on nanosecond time scale is too fast to be assigned to intrinsic deactivation of triplet excitons generated in organic molecules without heavy metals (Figure S4). Therefore, we speculate that the PL on the nanosecond time scale may be induced by the S_1 state repopulated through TTA. Another possible explanation for the slow PL may be the presence of highly ordered regions with a suppressed nonradiative decay rate in Y6 films. This is because (TR)PL measurements are dominated by emissive states, whereas TA measurements can directly probe the exciton density. This speculation originates from the fact that the peak positions of the GSB red-shift with time, suggesting the presence of highly ordered regions, where excitons are expected to decay more slowly with higher PL quantum yields owing to the suppressed nonradiative decay. This results in a change in the ratio of the TA amplitudes between the singlet PIA and SE. Further studies are required to reveal the origin of the slow PL. Nevertheless, what is important here is that the majority of the singlet

excitons decay with a time constant of 220 ps. Therefore, we chose 220 ps as the exciton lifetime of Y6 in the solid state for later discussion.

Singlet exciton diffusion. The diffusion properties of Y6 singlet excitons can be determined by analyzing the excitation-fluence-dependent kinetics of exciton decay.[33-35] The rate equation for singlet excitons, including SSA, is given by

$$\frac{\mathrm{d}n_{\mathrm{S}}(t)}{\mathrm{d}t} = -kn_{\mathrm{S}}(t) - \frac{1}{2}\gamma(t)n_{\mathrm{S}}(t)^2 \tag{1}$$

where $n_s(t)$, k, and $\gamma(t)$ are the singlet exciton density at time t after photoexcitation, the rate constant for monomolecular deactivation given by the inverse of the exciton lifetime (~220 ps for Y6 in the solid state), and the SSA rate coefficient, respectively (details are found in the Supporting Information). Equation 1 can be analytically solved as

$$n_{\mathrm{S}}(t) = \frac{n_0 \exp(-kt)}{1 + \frac{n_0}{2}G(t)} \tag{2}$$

$$G(t) = 8\pi DR\left[\frac{1}{k}(1 - e^{-kt}) + \frac{R}{\sqrt{2Dk}}\mathrm{erf}\left(\sqrt{kt}\right)\right] \tag{3}$$

where n_0 is the initial exciton density, and "erf" denotes the error function. Herein, we used a three-dimensionally (3D) isotropic diffusion model,[33-35] and the effective reaction radius R is assumed to be 1 nm as a typical value for small molecules to provide a straightforward comparison with previous studies.

Singlet excitons decay faster with increasing excitation fluence in the 70 nm thick Y6 film due to SSA. The red and blue lines in Figure 3 are best fits obtained using Equations 2 and 3 with and without the second term (the error function term) in Equation 3, respectively. Both fitting curves reproduce the experimentally observed exciton decay kinetics well, which is a sign of a relatively fast diffusion because the error function term is negligible when $t >> R^2/(2\pi D)$. From the fitting with the error function term (red line), D is evaluated to be 2.1×10^{-2} cm^2 s^{-1}. This value is approximately one order of magnitude larger than those of typical conjugated polymers[35] but similar to those of recent novel NFAs[21,36], wherein the authors claimed that the diffusion coefficients of NFA excitons are larger than that of donor polymers owing to their rigid planar molecular structures. L_D was calculated to be ~21 nm; this relatively long diffusion length is a key factor that determines efficient charge generation in Y6-based OSCs.

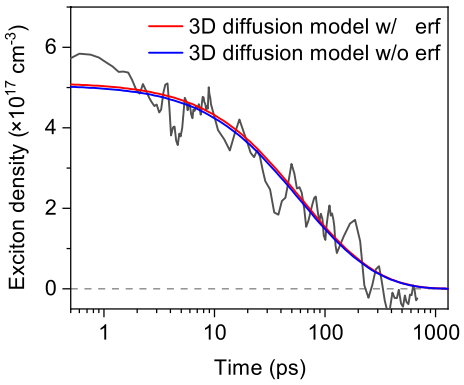

Figure 3. Singlet exciton decay kinetics for the 70 nm thick Y6 film monitored at 970 nm. The excitation wavelength was 800 nm with a fluence of 1.4 μJ cm^{-2}. The red and blue lines represent the best fits obtained using the 3D diffusion model with and without the error function term, respectively.

Triplet excited state energy of Y6. To determine E_{T1}, we acquired the PL spectra of a mixed solution of Y6 and rubrene after selectively exciting the lower-bandgap Y6. Figure 4a shows the

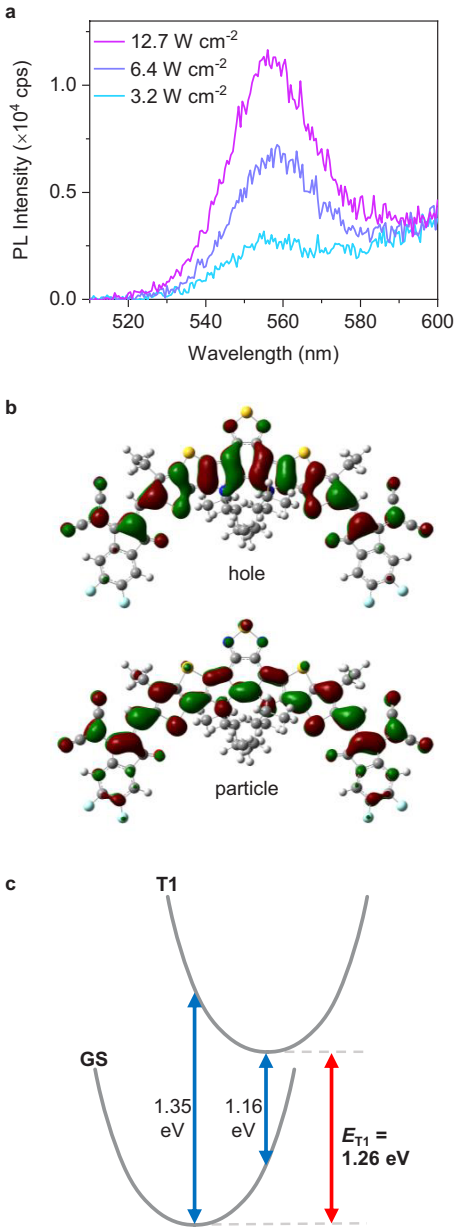

Figure 4. (a) UC emission spectra of a Y6/rubrene mixture in a CF solution (1.5 μM/300 μM) excited at 635 nm. (b) NTO pairs for Y6 in the optimized T_1 geometry obtained through TD-DFT calculations with B3LYP/6-31+G(d) within the Tamm–Dancoff approximation. (c) Schematic defining E_{T1}.

PL spectra of a mixed solution of Y6 (1.5 μM) and rubrene (300 μM). We observed an emission at ~560 nm, which is shorter than the excitation wavelength. As this emission band coincides with rubrene fluorescence,[37] we attribute it to the upconversion (UC) emission from rubrene. Upon photoexcitation of Y6, triplet excitons are generated through ISC. Then, triplet energy transfer from Y6 to rubrene occurs to form rubrene triplet excitons that diffuse randomly and undergo TTA when they encounter one another, resulting in the generation of rubrene singlet excitons with energy higher than the excitation source. The rubrene singlet excitons decay rapidly to the ground state by emitting upconverted photons; i.e., UC emission. E_{T1} of rubrene is 1.14 eV;[37] thus, E_{T1} of Y6 is higher than 1.14 eV. To confirm that this estimation is reliable, we carried out DFT calculations for an isolated Y6 molecule. Figure 4b shows the natural transition orbital (NTO)[38] pairs of Y6 in the optimized T_1 geometry obtained by TD-DFT calculations. E_{T1} was calculated to be 1.26 eV from the average of two vertical excitation energies at the optimized T_1 and ground state (GS) geometries (Figure 4c). Note that, in a previous study, UC emission from rubrene was also observed in a bilayer film consisting of rubrene and Y6,[39] which indicates that E_{T1} of Y6 in the solid state is also higher than that of rubrene. As the energy level of the S_1 state E_{S1} in the solid state was determined to be 1.39 eV (Figure S1), this means that the energy difference between the S_1 and T_1 states of Y6 in the solid state is less than 0.3 eV, which is considerably smaller than those of donor conjugated polymers (typically 0.5–0.7 eV). This small energy difference is probably due to the A-D-A′-D-A molecular architecture of Y6, which reduces the overlap between HOMO and the lowest unoccupied molecular orbital (LUMO), thereby lowering the exchange integral.

Ultrafast triplet generation through singlet fission following SSA

Figure 5 shows the TA spectra of the pristine Y6 film at a high excitation fluence. Interestingly, triplet PIA is more pronounced compared to that at lower excitation fluences. As shown in Figure 5c, the peak positions of the PIA bands at the longer wavelength region blue-shifts within the first 10 ps, indicating that singlet excitons are converted into triplet excitons in this fast time scale. Such ultrafast triplet formation was not observed in either Y6 in the CF solution or the pristine Y6 film at low excitation fluences. Therefore, the ultrafast triplet formation at high excitation fluences cannot be rationalized by ISC. To investigate the mechanism of ultrafast triplet formation at high excitation fluences, we examined the relationship between the TA signal and the excitation fluence. Figures 6a and 6b show log–log plots of the TA signal amplitudes monitored at 850 and 1400 nm, respectively; these plots are well fitted by the following power-law equation: $\Delta OD \propto I_{ex}^{m}$, where I_{ex} is the excitation fluence, and the slope m depends on the time duration after photoexcitation. Here, we provide a brief summary of the trends in the m value (detailed discussion can be found in the Supporting Information). For singlet excitons, the m value is unity when the SSA is negligible, whereas it decreases with increasing contribution of the SSA to the decay of singlet excitons, and finally approaches 0.5 when the SSA is the dominant decay channel. For triplet excitons, on the other hand, the m value is 0.5 or lower when the S_n state generated through SSA merely decays to the S_1 state and ISC is the only channel for triplet formation, whereas it is unity when the S_n state converts to triplet exciton before deactivation. As shown in Figure 6c, the slope of the 850 nm signal (GSB) decreased to 0.5 on early times, indicating that SSA is the dominant decay channel for Y6 singlet excitons at high excitation fluences. The slopes of the 850 nm signal recovered to unity after 500 ps, at which time triplet excitons are dominant as singlet excitons had completely decayed. Simultaneously, the slopes of the 1400 nm at later times are also unity. These results indicate that triplet excitons are generated through the S_n state via SSA at high excitation

fluences. Figure 6d shows the decay kinetics of Y6 triplet excitons generated through SSA; these

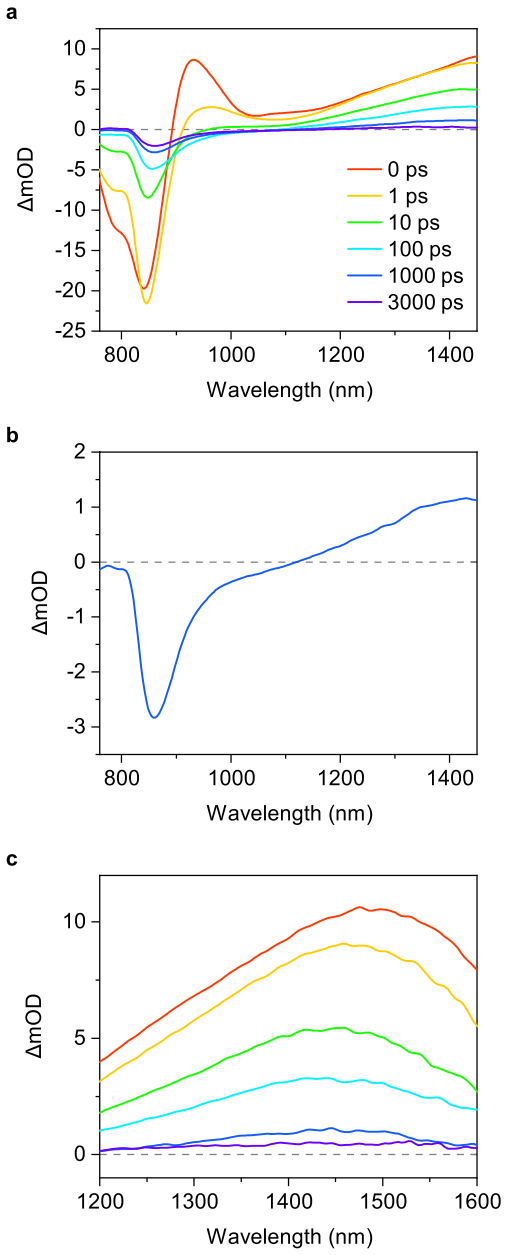

Figure 5. (a) TA spectra of the pristine Y6 film. The excitation wavelength was 800 nm with a fluence of 31.1 μJ cm^{-2}. (b) Enlarged TA spectra at 1000 ps. (c) TA spectra at the longer wavelength region obtained by using an appropriate long-pass filter to avoid detection of second-order diffraction of shorter wavelengths. Color legends in figures (b) and (c) are the same as those of (a).

excitons decay quickly on nanosecond time scale, which is too fast to be assigned to the intrinsic Y6 triplet exciton decay as it should be on the order of microsecond (Figure S3). Interestingly, the decay dynamics of the Y6 triplet excitons generated through SSA are almost independent of the excitation fluence. Such a fluence-independent fast triplet decay has been reported for some singlet fission materials, wherein triplet pairs generated through singlet fission decay geminately before they dissociate into two free triplets.[40,41] This is consistent with the observation of SE in the 900–1100 nm region on the nanosecond time scale, as shown in Figures 5, which indicates that the triplet pairs recombine to the S_1 state, followed by delayed fluorescence. Thus, we conclude that

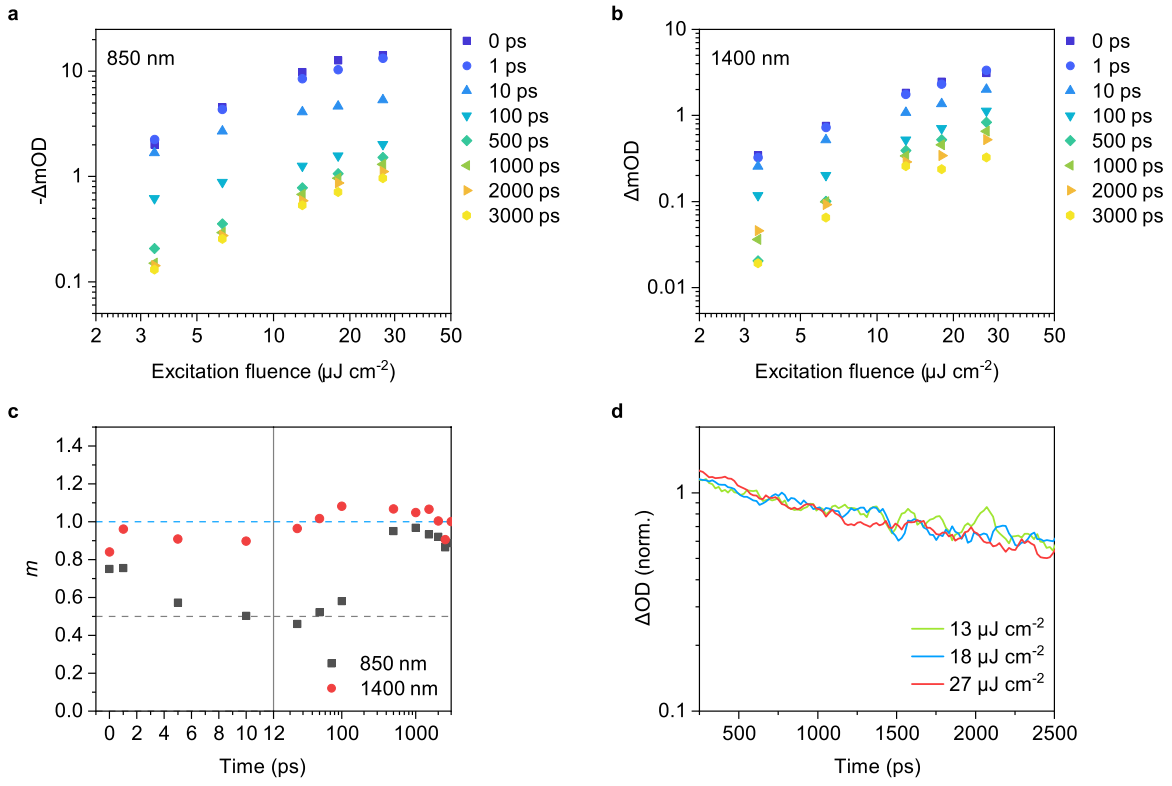

Figure 6. (a,b) Log–log plots of the TA signals monitored at (a) 850 nm and (b) 1400 nm. (c) Time evolution of the slope *m*. Two broken lines represent 1 (blue) and 0.5 (gray) as a guide for the eye. (d) Excitation-fluence dependence of Y6 triplet decay at higher excitation fluences.

ultrafast formation of triplet excitons observed at high excitation fluences can be rationalized by singlet fission from the S_n states generated by SSA. As the S_n state generated by SSA possesses twice as much energy as the S_1 state, the S_n state always satisfies the energetic requirement for singlet fission; i.e., $E_S > 2E_T$.[42] This process has been reported for anthracene for the first time,[42] as well as for some conjugated polymers.[40,41] This result also implies that the slow PL decay mentioned in the previous section may be a result of the geminate recombination of the triplet pairs instead of free triplet excitons because the S_n states can also be generated after the 400 nm excitation without SSA.[41,43]

Conclusions

We have studied the singlet and triplet excited-state dynamics of Y6 in the solid state. We found that singlet excitons in pristine Y6 films exhibit biphasic decay kinetics with decay constants of ~220 ps and ~1200 ps. The majority of the Y6 singlet excitons decayed with the faster (~220 ps) component, whereas the Y6 films continued to exhibit PL on the nanosecond time scale despite the absence of singlet PIA on the nanosecond time scale. Accordingly, we speculate that the slow PL may be induced by the S_1 state repopulated through TTA of free triplet excitons or geminate recombination of triplet pairs following singlet fission. We also speculate the possible presence of highly ordered regions with a suppressed nonradiative decay rate in the pristine Y6 films. Y6 exhibits relatively fast singlet exciton diffusion with a diffusion constant of 2.1×10^{-2} cm^2 s^{-1}, which is crucial for efficient photocurrent generation in Y6-based OSCs. Fast singlet exciton diffusion easily causes SSA at high excitation fluences. The S_n states generated by SSA undergo singlet fission to form triplet pairs in competition with vibrational relaxation to the S_1 state. Although SSA-mediated singlet fission does not improve the PCE of OSCs because it generates

two triplet excitons from two singlet excitons, the observation of singlet fission from the S_n states highlights the potential application of Y6 as a photon multiplier because the S_n states can also be generated by irradiation with UV–visible light. The small (<0.3 eV) energy difference between the S_1 and T_1 states of Y6 in the solid state is another important property. Because the energy level of the T_1 state is a critical factor governing the bimolecular charge recombination rate in OSCs, the small S_1–T_1 energy difference is the key to further improve Y6-based OSCs.

ASSOCIATED CONTENT

Supporting Information

Supporting Information is available free of charge via the Internet at http://pubs.acs.org.

Chemical structure of Y6; steady-state absorption and PL spectra; assignment of Y6 singlet excitons; assignment of Y6 triplet excitons; Triplet PIA on the microsecond time scale; TA spectra of the 240 nm thick Y6 film; PL decay; details of SSA model; details of excitation-fluence dependence

AUTHOR INFORMATION

Corresponding Author

Yasunari Tamai

Department of Polymer Chemistry, Graduate School of Engineering, Kyoto University, Katsura, Nishikyo, Kyoto 615-8510, Japan; Japan Science and Technology Agency (JST), PRESTO, 4-1-8 Honcho Kawaguchi, Saitama 332-0012, Japan; ORCID: 0000-0002-3074-0208; Email: tamai@photo.polym.kyoto-u.ac.jp

Author Contributions

YT conceived and directed the project. SN, YS, RS and TS performed steady-state and time-resolved optical measurements under the supervision of YT. SN, TT and YT analyzed time-resolved data. SN and YT prepared the original version of the manuscript. All authors have given approval to the final version of the manuscript.

Notes

The authors declare no competing financial interests.

ACKNOWLEDGMENTS

This study was partly supported by the JST PRESTO program Grant Number JPMJPR1874, JSPS KAKENHI Grant-in-Aid for Scientific Research (B) No. 21H02012, The Murata Science Foundation, The Sumitomo Foundation, and Ogasawara Toshiaki Memorial Foundation.

ORCID (co-authors)

Hideo Ohkita: 0000-0002-7403-3492

References

1. Liu, Q.; Jiang, Y.; Jin, K.; Qin, J.; Xu, J.; Li, W.; Xiong, J.; Liu, J.; Xiao, Z.; Sun, K. et al. 18% Efficiency Organic Solar Cells. *Sci. Bull.* **2020,** *65*, 272-275.

2. Liu, F.; Zhou, L.; Liu, W.; Zhou, Z.; Yue, Q.; Zheng, W.; Sun, R.; Liu, W.; Xu, S.; Fan, H. et al. Organic Solar Cells with 18% Efficiency Enabled by an Alloy Acceptor: A Two-in-One Strategy. *Adv. Mater.* **2021,** *33*, 2100830.

3. Zhang, M.; Zhu, L.; Zhou, G.; Hao, T.; Qiu, C.; Zhao, Z.; Hu, Q.; Larson, B. W.; Zhu, H.; Ma, Z. et al. Single-Layered Organic Photovoltaics with Double Cascading Charge Transport Pathways: 18% Efficiencies. *Nat. Commun.* **2021,** *12*, 309.

4. Tamai, Y.; Fan, Y.; Kim, V. O.; Ziabrev, K.; Rao, A.; Barlow, S.; Marder, S. R.; Friend, R. H.; Menke, S. M. Ultrafast Long-Range Charge Separation in Nonfullerene Organic Solar Cells. *ACS Nano* **2017,** *11*, 12473-12481.

5. Hou, J.; Inganäs, O.; Friend, R. H.; Gao, F. Organic Solar Cells Based on Non-Fullerene Acceptors. *Nat. Mater.* **2018,** *17*, 119-128.

6. Zhang, G. Y.; Zhao, J. B.; Chow, P. C. Y.; Jiang, K.; Zhang, J. Q.; Zhu, Z. L.; Zhang, J.; Huang, F.; Yan, H. Nonfullerene Acceptor Molecules for Bulk Heterojunction Organic Solar Cells. *Chem. Rev.* **2018,** *118*, 3447-3507.

7. Wadsworth, A.; Moser, M.; Marks, A.; Little, M. S.; Gasparini, N.; Brabec, C. J.; Baran, D.; McCulloch, I. Critical Review of the Molecular Design Progress in Non-Fullerene Electron Acceptors Towards Commercially Viable Organic Solar Cells. *Chem. Soc. Rev.* **2019,** *48*, 1596-1625.

8. Cui, Y.; Yao, H. F.; Zhang, J. Q.; Zhang, T.; Wang, Y. M.; Hong, L.; Xian, K. H.; Xu, B. W.; Zhang, S. Q.; Peng, J. et al. Over 16% Efficiency Organic Photovoltaic Cells Enabled by a Chlorinated Acceptor with Increased Open-Circuit Voltages. *Nat. Commun.* **2019,** *10*, 8.

9. Yuan, J.; Zhang, Y. Q.; Zhou, L. Y.; Zhang, G. C.; Yip, H. L.; Lau, T. K.; Lu, X. H.; Zhu, C.; Peng, H. J.; Johnson, P. A. et al. Single-Junction Organic Solar Cell with over 15% Efficiency Using Fused-Ring Acceptor with Electron-Deficient Core. *Joule* **2019,** *3*, 1140-1151.

10. Saito, T.; Natsuda, S.-i.; Imakita, K.; Tamai, Y.; Ohkita, H. Role of Energy Offset in Nonradiative Voltage Loss in Organic Solar Cells. *Sol. RRL* **2020,** *4*, 2000255.

11. Umeyama, T.; Igarashi, K.; Sasada, D.; Tamai, Y.; Ishida, K.; Koganezawa, T.; Ohtani, S.; Tanaka, K.; Ohkita, H.; Imahori, H. Efficient Light-Harvesting, Energy Migration, and Charge Transfer by Nanographene-Based Nonfullerene Small-Molecule Acceptors Exhibiting Unusually Long Excited-State Lifetime in the Film State. *Chem. Sci.* **2020,** *11*, 3250-3257.

12. Armin, A.; Li, W.; Sandberg, O. J.; Xiao, Z.; Ding, L.; Nelson, J.; Neher, D.; Vandewal, K.; Shoaee, S.; Wang, T. et al. A History and Perspective of Non-Fullerene Electron Acceptors for Organic Solar Cells. *Adv. Energy Mater.* **2021,** *11*, 2003570.

13. Karki, A.; Vollbrecht, J.; Dixon, A. L.; Schopp, N.; Schrock, M.; Reddy, G. N. M.; Nguyen, T.-Q. Understanding the High Performance of over 15% Efficiency in Single-Junction Bulk Heterojunction Organic Solar Cells. *Adv. Mater.* **2019,** *31*, 1903868.

14. Hosseini, S. M.; Tokmoldin, N.; Lee, Y. W.; Zou, Y.; Woo, H. Y.; Neher, D.; Shoaee, S. Putting Order into PM6:Y6 Solar Cells to Reduce the Langevin Recombination in 400 nm Thick Junction. *Sol. RRL* **2020,** *4*, 2000498.

15. Tokmoldin, N.; Hosseini, S. M.; Raoufi, M.; Phuong, L. Q.; Sandberg, O. J.; Guan, H.; Zou, Y.; Neher, D.; Shoaee, S. Extraordinarily Long Diffusion Length in PM6:Y6 Organic Solar Cells. *J. Mater. Chem. A* **2020,** *8*, 7854-7860.

16. Perdigón-Toro, L.; Zhang, H.; Markina, A.; Yuan, J.; Hosseini, S. M.; Wolff, C. M.; Zuo, G.; Stolterfoht, M.; Zou, Y.; Gao, F. et al. Barrierless Free Charge Generation in the High-Performance PM6:Y6 Bulk Heterojunction Non-Fullerene Solar Cell. *Adv. Mater.* **2020,** *32*, 1906763.

17. Zhu, W.; Spencer, A. P.; Mukherjee, S.; Alzola, J. M.; Sangwan, V. K.; Amsterdam, S. H.; Swick, S. M.; Jones, L. O.; Heiber, M. C.; Herzing, A. A. et al. Crystallography, Morphology, Electronic Structure, and Transport in Non-Fullerene/Non-Indacenodithienothiophene Polymer:Y6 Solar Cells. *J. Am. Chem. Soc.* **2020,** *142*, 14532-14547.

18. Zhang, G.; Chen, X.-K.; Xiao, J.; Chow, P. C. Y.; Ren, M.; Kupgan, G.; Jiao, X.; Chan, C. C. S.; Du, X.; Xia, R. et al. Delocalization of Exciton and Electron Wavefunction in Non-Fullerene Acceptor Molecules Enables Efficient Organic Solar Cells. *Nat. Commun.* **2020,** *11*, 3943.

19. Tokmoldin, N.; Vollbrecht, J.; Hosseini, S. M.; Sun, B.; Perdigón-Toro, L.; Woo, H. Y.; Zou, Y.; Neher, D.; Shoaee, S. Explaining the Fill-Factor and Photocurrent Losses of Nonfullerene Acceptor-Based Solar Cells by Probing the Long-Range Charge Carrier Diffusion and Drift Lengths. *Adv. Energy Mater.* **2021,** *11*, 2100804.

20. Wu, J.; Lee, J.; Chin, Y.-C.; Yao, H.; Cha, H.; Luke, J.; Hou, J.; Kim, J.-S.; Durrant, J. R. Exceptionally Low Charge Trapping Enables Highly Efficient Organic Bulk Heterojunction Solar Cells. *Energy Environ. Sci.* **2020,** *13*, 2422-2430.

21. Firdaus, Y.; Le Corre, V. M.; Karuthedath, S.; Liu, W.; Markina, A.; Huang, W.; Chattopadhyay, S.; Nahid, M. M.; Nugraha, M. I.; Lin, Y. et al. Long-Range Exciton Diffusion in Molecular Non-Fullerene Acceptors. *Nat. Commun.* **2020,** *11*, 5220.

22. Classen, A.; Chochos, C. L.; Lüer, L.; Gregoriou, V. G.; Wortmann, J.; Osvet, A.; Forberich, K.; McCulloch, I.; Heumüller, T.; Brabec, C. J. The Role of Exciton Lifetime for Charge Generation in Organic Solar Cells at Negligible Energy-Level Offsets. *Nat. Energy* **2020,** *5*, 711-719.

23. Zhan, L.; Li, S.; Lau, T.-K.; Cui, Y.; Lu, X.; Shi, M.; Li, C.-Z.; Li, H.; Hou, J.; Chen, H. Over 17% Efficiency Ternary Organic Solar Cells Enabled by Two Non-Fullerene Acceptors Working in an Alloy-Like Model. *Energy Environ. Sci.* **2020,** *13*, 635-645.

24. Wen, G.; Hu, R.; Su, X.; Chen, Z.; Zhang, C.; Peng, J.; Zou, X.; He, X.; Dong, G.; Zhang, W. Excited-State Properties of Y-Series Small Molecule Semiconductors. *Dyes and Pigments* **2021,** *192*, 109431.

25. Liang, S.; Li, S.; Zhang, Y.; Li, T.; Zhou, H.; Jin, F.; Sheng, C.; Ni, G.; Yuan, J.; Ma, W. et al. Efficient Hole Transfer via Delocalized Excited State in Small Molecular Acceptor: A Comparative Study on Photodynamics of PM6:Y6 and PM6:ITIC Organic Photovoltaic Blends. *Adv. Funct. Mater.* **2021,** *31*, 2102764.

26. Wang, R.; Xu, J.; Fu, L.; Zhang, C.; Li, Q.; Yao, J.; Li, X.; Sun, C.; Zhang, Z.-G.; Wang, X. et al. Nonradiative Triplet Loss Suppressed in Organic Photovoltaic Blends with Fluoridated Nonfullerene Acceptors. *J. Am. Chem. Soc.* **2021,** *143*, 4359-4366.

27. Chow, P. C. Y.; Chan, C. C. S.; Ma, C.; Zou, X.; Yan, H.; Wong, K. S. Factors That Prevent Spin-Triplet Recombination in Non-Fullerene Organic Photovoltaics. *J. Phys. Chem. Lett.* **2021,** *12*, 5045-5051.

28. Ohkita, H.; Tamai, Y.; Benten, H.; Ito, S. Transient Absorption Spectroscopy for Polymer Solar Cells. *IEEE J. Sel. Top. Quantum Electron.* **2016,** *22*, 100-111.

29. Frisch, M. J.; Trucks, G. W.; Schlegel, H. B.; Scuseria, G. E.; Robb, M. A.; Cheeseman, J. R.; Scalmani, G.; Barone, V.; Petersson, G. A.; Nakatsuji, H. et al. *Gaussian 16 Rev. A.01*, Wallingford, CT, 2016.

30. Peach, M. J. G.; Williamson, M. J.; Tozer, D. J. Influence of Triplet Instabilities in Tddft. *J. Chem. Theory Comput.* **2011,** *7*, 3578-3585.

31. Karki, A.; Vollbrecht, J.; Gillett, A. J.; Xiao, S. S.; Yang, Y.; Peng, Z.; Schopp, N.; Dixon, A. L.; Yoon, S.; Schrock, M. et al. The Role of Bulk and Interfacial Morphology in Charge Generation, Recombination, and Extraction in Non-Fullerene Acceptor Organic Solar Cells. *Energy Environ. Sci.* **2020,** *13*, 3679-3692.

32. Sakamoto, Y.; Tamai, Y.; Ohkita, H. Sensitizer-Host-Annihilator Ternary-Cascaded Triplet Energy Landscape for Efficient Photon Upconversion in the Solid State. *J Chem Phys* **2020,** *153*, 161102.

33. Tamai, Y.; Matsuura, Y.; Ohkita, H.; Benten, H.; Ito, S. One-Dimensional Singlet Exciton Diffusion in Poly(3-hexylthiophene) Crystalline Domains. *J. Phys. Chem. Lett.* **2014,** *5*, 399-403.

34. Murata, Y.; Takeyama, T.; Sakamoto, Y.; Yamaguchi, K.; Tamai, Y.; Ohkita, H. Two-Dimensional Exciton Diffusion in an HJ-Aggregate of Naphthobisoxadiazole-Based Copolymer Films. *J. Phys. Chem. C* **2020,** *124*, 13063-13070.

35. Tamai, Y.; Ohkita, H.; Benten, H.; Ito, S. Exciton Diffusion in Conjugated Polymers: From Fundamental Understanding to Improvement in Photovoltaic Conversion Efficiency. *J. Phys. Chem. Lett.* **2015,** *6*, 3417-3428.

36. Chandrabose, S.; Chen, K.; Barker, A. J.; Sutton, J. J.; Prasad, S. K. K.; Zhu, J.; Zhou, J.; Gordon, K. C.; Xie, Z.; Zhan, X. et al. High Exciton Diffusion Coefficients in Fused Ring Electron Acceptor Films. *J. Am. Chem. Soc.* **2019,** *141*, 6922-6929.

37. Ma, L.; Zhang, K.; Kloc, C.; Sun, H.; Michel-Beyerle, M. E.; Gurzadyan, G. G. Singlet Fission in Rubrene Single Crystal: Direct Observation by Femtosecond Pump–Probe Spectroscopy. *Phys. Chem. Chem. Phys.* **2012,** *14*, 8307-8312.

38. Martin, R. L. Natural Transition Orbitals. *J. Chem. Phys.* **2003,** *118*, 4775-4777.

39. Izawa, S.; Hiramoto, M. Efficient Solid-State Photon Upconversion Enabled by Spin Inversion at Organic Semiconductor Interface. *ChemRxiv*, 2021, DOI: 10.26434/chemrxiv.14184830.v1.

40. Tamai, Y.; Ohkita, H.; Benten, H.; Ito, S. Singlet Fission in Poly(9,9-di-*n*-octylfluorene) Films. *J. Phys. Chem. C* **2013,** *117*, 10277-10284.

41. Kasai, Y.; Tamai, Y.; Ohkita, H.; Benten, H.; Ito, S. Ultrafast Singlet Fission in a Push-Pull Low-Bandgap Polymer Film. *J Am Chem Soc* **2015,** *137*, 15980-15983.

42. Smith, M. B.; Michl, J. Singlet Fission. *Chem. Rev.* **2010,** *110*, 6891-6936.

43. Musser, A. J.; Al-Hashimi, M.; Maiuri, M.; Brida, D.; Heeney, M.; Cerullo, G.; Friend, R. H.; Clark, J. Activated Singlet Exciton Fission in a Semiconducting Polymer. *J. Am. Chem. Soc.* **2013,** *135*, 12747-12754.

Supporting Information for

Singlet and Triplet Excited-State Dynamics of a Nonfullerene Electron Acceptor Y6

Shin-ichiro Natsuda[1], *Yuji Sakamoto*[1], *Taiki Takeyama*[1], *Rei Shirouchi*[1], *Toshiharu Saito*[1], *Yasunari Tamai*[1,2*], *Hideo Ohkita*[1]

[1] Department of Polymer Chemistry, Graduate School of Engineering, Kyoto University, Katsura, Nishikyo, Kyoto 615-8510, Japan

[2] Japan Science and Technology Agency (JST), PRESTO, 4-1-8 Honcho Kawaguchi, Saitama 332-0012, Japan

[*]to whom correspondence: tamai@photo.polym.kyoto-u.ac.jp

Steady-state absorption and PL spectra

E_{S1} for Y6 in a CF solution and the pristineY6 film were determined to be 1.64 and 1.39 eV, respectively, from the intersection of the absorption and PL spectra. PLQY of the pristine Y6 film was evaluated to be 4.3%.

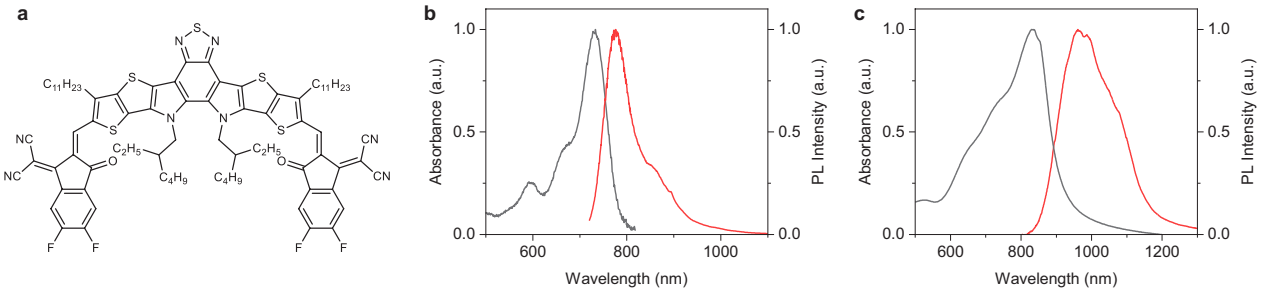

Figure S1. (a) Chemical structure of Y6. (b) Absorption (gray) and PL (red) spectra of Y6 in a CF solution. (c) Absorption (gray) and PL (red) spectra of the pristine Y6 film.

Assignment of Y6 singlet excitons

Figure S2a shows the TA spectra of Y6 in a CF solution. A large PIA band at ~900 nm and a broad PIA tail above 1200 nm appeared immediately after photoexcitation. The decay kinetics monitored at 900 nm were independent of the excitation fluence (Figure S2b), indicating negligible bimolecular decay processes, such as SSA. The main decay component is well reproduced with an exponential function, as shown by the blue line. The decay time constant was ~1000 ps, which is in good agreement with the PL lifetime (Figure S6a), indicating that this PIA can be assigned to Y6 singlet excitons. In addition, the time profile displays a relatively fast decay component (~4.0 ps), which is attributable to the change in the absorption cross-section of Y6 singlet excitons, probably owing to the structural change in the excited state. Such a fast TA signal decay has been observed in other NFAs, such as ITIC.[S1,S2] The decay kinetics at 1400 nm are largely coincident with those at 900 nm; the former band can be well fitted by a sum of the same exponential function and a constant fraction. This means that the broad tail above 1200 nm at early times can also be assigned to Y6 singlet excitons. The constant fraction observed at later times can be assigned to Y6 triplet excitons formed through ISC, as shown in Figure S3.

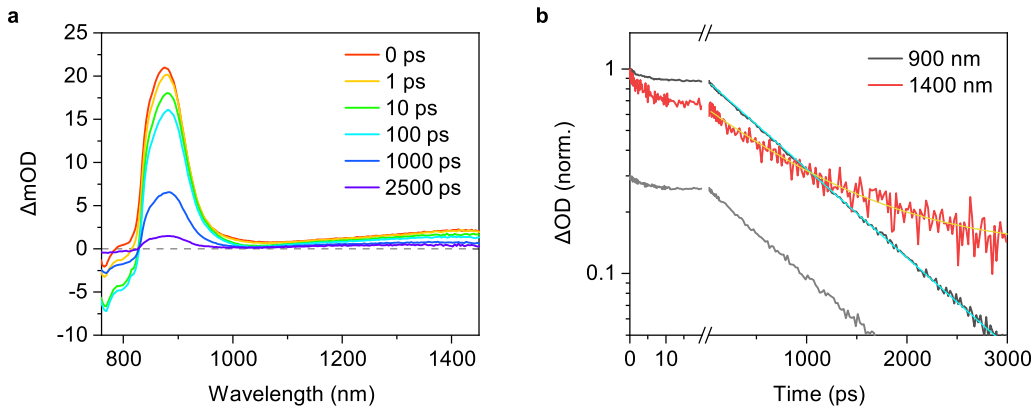

Figure S2. (a) TA spectra of Y6 in a CF solution. The excitation wavelength was set to 700 nm with a fluence of 72 μJ cm^{-2}. (b) Decay kinetics monitored at 900 nm (black) and 1400 nm (red). The gray line represents the decay kinetics at 900 nm measured at a weak excitation fluence of 29 μJ cm^{-2}. The 900 nm curve was well fitted by an exponential function with a time constant of 1000 ps (blue line). The 1400 nm curve was well fitted by a sum of the same exponential function and a constant fraction (yellow line). The constant fraction corresponds to Y6 triplet excitons generated through ISC.

Assignment of Y6 triplet excitons

Figure S3 shows the TA spectra of Y6 in a CF solution on microsecond time scale. A long-lived PIA band was observed at 1300 nm, which is identical to that observed on nanosecond time scale, as shown in Figure S2. This band decayed monoexponentially with a time constant of 31.5 μs in a N_2 atmosphere and decayed significantly faster in an O_2 atmosphere (Figure S3b), indicating that the PIA band can be assigned to the T_1–T_n absorption of Y6.

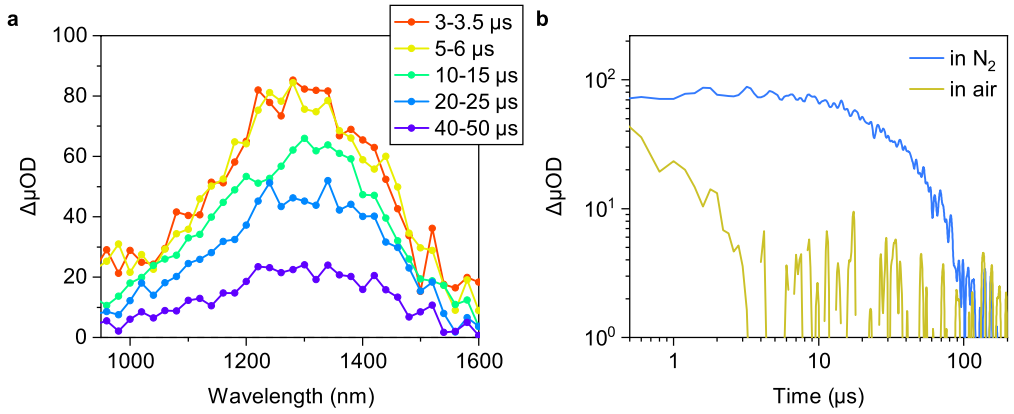

Figure S3. (a) TA spectra of Y6 in a CF solution. The excitation wavelength was set to 532 nm with a fluence of 8.6 μJ cm^{-2}. (b) Time evolution of TA signals monitored at 1300 nm under N_2 or ambient conditions.

Triplet PIA on the microsecond time scale

In the solid state, triplet excitons decayed significantly faster than that in the CF solution (Figure S3). Thus, the lifetime of Y6 triplets in the solid state cannot be determined due to the limitation of the time resolution of our TA setup. Instead, a large negative signal was observed in the <1200 nm region. This negative signal is attributable to the delayed fluorescence from Y6 following TTA, which is suggestive of fast diffusion of Y6 triplet excitons in the solid state.

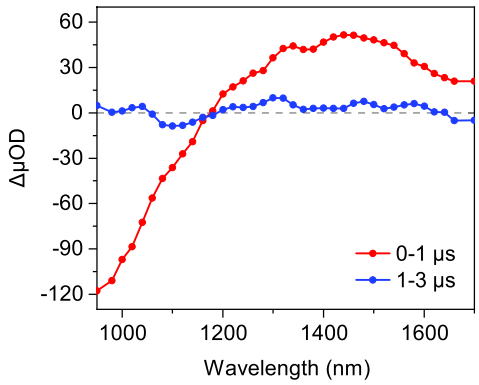

Figure S4. TA spectra of the Y6/PtOEP blend film averaged over 0–1 μs (red) and 1–3 μs (blue). The excitation wavelength was set to 532 nm with a fluence of 9.4 μJ cm^{-2}.

TA spectra of the 240 nm thick Y6 film

Figure S5 shows the TA spectra of the 240 nm thick Y6 film. The singlet exciton absorption was observed immediately after photoexcitation, as in the case of the 70 nm thick Y6 film (Figure 1a). Note that the peak ratio between the singlet PIA and GSB in the thick Y6 film is different from that of the thin Y6 film. A possible explanation is that the SE is weaker in the thick Y6 film because of self-absorption of the emitted photons, thereby mitigating the spectral overlap between positive PIA and negative SE in this spectral region. This results in a relatively larger positive PIA in the thick Y6 film.

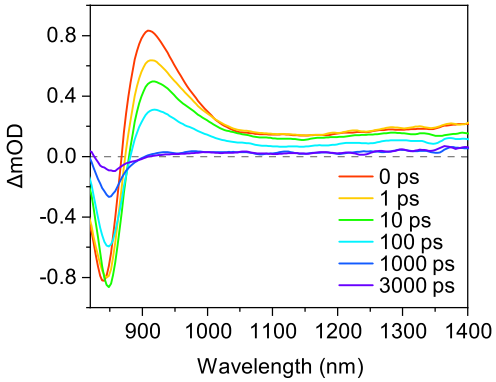

Figure S5. TA spectra of the 240 nm thick Y6 film. The excitation wavelength was set to 400 nm with a fluence of 3.0 μJ cm^{-2}.

PL decay

For Y6 films, we measured the PL decay kinetics using two different detectors. One had an instrumental response function (IRF) of ~280 ps (fwhm) but could not measure the >800 nm region (Figure S6b), and the other had an IRF of ~1.1 ns but could measure the >800 nm region (Figure S6c). Regardless of the detector, we obtained the same PL lifetime of 1.2 ns.

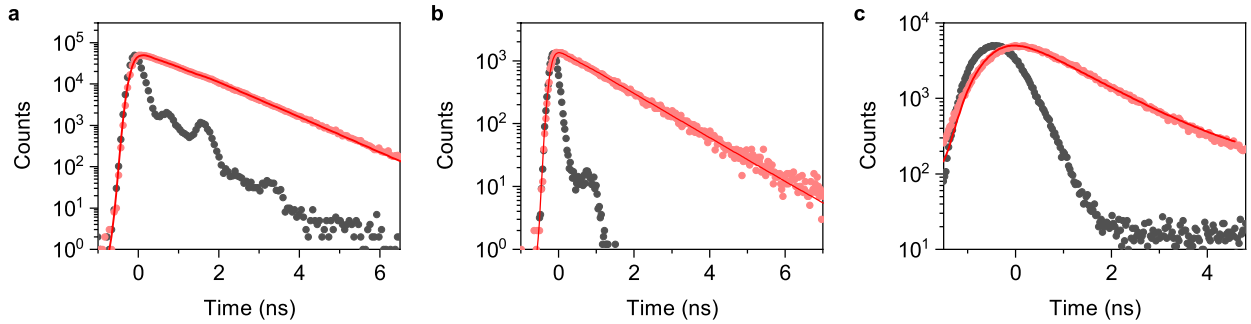

Figure S6. (a) PL decay kinetics of Y6 in a CF solution (red circles) measured by the TCSPC method. The gray circles show the IRF (fwhm ~280 ps). The excitation and detection wavelengths were 640 nm and 770 nm, respectively. The decay kinetics are well reproduced by a convolution of the IRF and an exponential function with a time constant of 1.0 ns (red line). (b,c) PL decay kinetics of a pristine Y6 film (red circles) measured by the TCSPC method. The gray circles show the IRF (fwhm (b): ~280 ps, (c): ~1.1 ns). The excitation wavelengths were 640 and 676 nm, respectively. Detection wavelengths were 800 and 920 nm, respectively. The decay kinetics are well reproduced by a convolution of the IRF and an exponential function with a time constant of 1.2 ns (red lines).

Details of SSA model

The rate equation for singlet excitons including SSA is given as

$$\frac{\mathrm{d}n_{\mathrm{S}}(t)}{\mathrm{d}t} = -kn_{\mathrm{S}}(t) - f\gamma(t){n_{\mathrm{S}}}^2(t) \tag{S1}$$

where $n_s(t)$, k, and $\gamma(t)$ are the singlet exciton density at time t after photoexcitation, the rate constant of monomolecular deactivation given by the inverse of the exciton lifetime (~220 ps for Y6 in the solid state), and the rate coefficient of SSA, respectively. Prefactor f depends on the exciton dynamics after SSA. The prefactor is 1/2 when the S_n state merely relaxes to the S_1 state ($S_1 + S_1 \rightarrow S_n + S_0 \rightarrow S_1 + S_0$ + phonons). On the other hand, f is unity if no singlet exciton remains after SSA (e.g., the S_n is converted into charged species or triplet excitons before vibrational relaxation to the S_1 state, $S_1 + S_1 \rightarrow S_n + S_0 \rightarrow$ charges or triplet excitons). Here, we assumed f = 1/2. Equation S1 can be analytically solved as

$$n_{\mathrm{S}}(t) = \frac{n_0 \exp(-kt)}{1 + \frac{n_0}{2} G(t)} \tag{S2}$$

$$G(t) = \int_0^t \gamma(t)\exp(-kt)\mathrm{d}t \tag{S3}$$

where n_0 represents the initial exciton density. Because SSA is a diffusion-limited process, the rate coefficient $\gamma(t)$ strongly depends on the diffusion properties of the excitons. Diffusion-limited bimolecular reaction rates are well known to depend significantly on the dimensionality of the system. The details are summarized in our previous studies.[S3-S5] Herein, we used a three-dimensionally (3D) isotropic diffusion model, wherein $\gamma(t)$ is given by

$$\gamma_{3\mathrm{D}}(t) = 8\pi DR\left(1 + \frac{R}{\sqrt{2\pi Dt}}\right) \tag{S4}$$

The effective reaction radius R is assumed to be 1 nm as a typical value for small molecules to provide a straightforward comparison with previous studies. Substituting Equation S4 into S3 gives

$$G(t) = 8\pi DR\left[\frac{1}{k}\left(1 - e^{-kt}\right) + \frac{R}{\sqrt{2Dk}}\mathrm{erf}\left(\sqrt{kt}\right)\right] \tag{S5}$$

where "erf" denotes the error function.

Details of excitation-fluence dependence

In the case of CW excitation, the steady-state condition is fulfilled. Although the steady-state approximation is not valid for pulse excitation, it is worthwhile to show the solution of rate equations for singlet and triplet excitons under steady-state conditions to understand the meaning of Figure 6.

Under steady-state conditions, a rate equation for singlet excitons is given as

$$\alpha I_{\mathrm{ex}} - k n_{\mathrm{S}} - f\gamma {n_{\mathrm{S}}}^2 = 0 \tag{S6}$$

where α and I_{ex} are the absorption coefficient at an excitation wavelength and excitation fluence, respectively. The meanings of the other symbols are the same as those described in the previous section.

We can assume $k >> f\gamma n_s$ at a low excitation fluence. In this case, n_s is given as

$$n_{\mathrm{S}} = \frac{\alpha I_{\mathrm{ex}}}{k} \propto I_{\mathrm{ex}} \tag{S7}$$

At a high excitation fluence, on the other hand, we can assume $k << f\gamma n_s$. In this case, n_s is given as

$$n_{\mathrm{S}} = \sqrt{\frac{\alpha I_{\mathrm{ex}}}{f\gamma}} \propto {I_{\mathrm{ex}}}^{0.5} \tag{S8}$$

Therefore, a decrease in the *m* value for the 850 nm (GSB) signals to 0.5 at early times, as shown in Figure 6c, indicates that SSA is the dominant decay channel for singlet excitons at high excitation fluences.

Similarly, a rate equation for triplet excitons under steady-state conditions is given as

$$k_{\mathrm{ISC}} n_{\mathrm{S}} + \Phi_{\mathrm{SF}} \gamma {n_{\mathrm{S}}}^2 - k_{\mathrm{TT}} n_{\mathrm{TT}} - k_{\mathrm{T}} n_{\mathrm{T}} - f_{\mathrm{TTA}} \gamma_{\mathrm{TTA}} {n_{\mathrm{T}}}^2 = 0 \tag{S9}$$

where k_{ISC}, Φ_{SF}, k_{TT}, n_{TT}, k_T, n_T, and γ_{TTA} are the rate constant of ISC, QY of singlet fission from the S_n state, the rate constant of geminate recombination for a triplet pair, the density of triplet pairs, the rate constant of monomolecular decay of free triplet excitons, the density of free triplet excitons, and the rate coefficient of TTA, respectively. The prefactor f_{TTA} represents the fraction of triplet excitons decaying after a TTA event. The first and second terms on the left-hand side of Equation S9 describe triplet generation through ISC from the S_1 state and through singlet fission from the S_n state, respectively. The third term represents geminate recombination of triplet pairs, whereas the fourth and fifth terms describe the decay of free triplet excitons through monomolecular and bimolecular (TTA) channels, respectively. If triplet generation through singlet fission is negligible (Φ_{SF} ~0) under a high excitation fluence, we will get

$$n_{\mathrm{T}} = \frac{k_{\mathrm{ISC}}}{k_{\mathrm{T}}}\sqrt{\frac{\alpha I_{\mathrm{ex}}}{f\gamma}} \propto {I_{\mathrm{ex}}}^{0.5} \tag{S10}$$

where we assumed that monomolecular deactivation is the dominant decay channel for triplet excitons. Note that we will get $m < 0.5$ if TTA contribute to the decay of triplet excitons.

On the other hand, when singlet fission is the main channel for triplet generation under a high excitation fluence, we will get

$$n_{\mathrm{TT}} = \frac{\alpha\Phi_{\mathrm{SF}}}{f k_{\mathrm{TT}}} I_{\mathrm{ex}} \propto I_{\mathrm{ex}} \tag{S11}$$

where for simplicity, we assumed that geminate recombination of triplet pairs is the dominant decay channel. Therefore, the m value of 1 for both the 850 and 1400 nm signals at later times indicates that triplet excitons at high excitation fluences are generated through singlet fission from the S_n states.

References

S1. Umeyama, T.; Igarashi, K.; Sasada, D.; Tamai, Y.; Ishida, K.; Koganezawa, T.; Ohtani, S.; Tanaka, K.; Ohkita, H.; Imahori, H. Efficient Light-Harvesting, Energy Migration, and Charge Transfer by Nanographene-Based Nonfullerene Small-Molecule Acceptors Exhibiting Unusually Long Excited-State Lifetime in the Film State. *Chem. Sci.* **2020,** *11*, 3250-3257.

S2. Umeyama, T.; Igarashi, K.; Tamai, Y.; Wada, T.; Takeyama, T.; Sasada, D.; Ishida, K.; Koganezawa, T.; Ohtani, S.; Tanaka, K.; Ohkita, H.; Imahori, H. Prolongation of the Singlet Exciton Lifetime of Nonfullerene Acceptor Films by the Replacement of the Central Benzene Core with Naphthalene. *Sustain. Energy Fuels* **2021,** *5*, 2028-2035.

S3. Tamai, Y.; Matsuura, Y.; Ohkita, H.; Benten, H.; Ito, S. One-Dimensional Singlet Exciton Diffusion in Poly(3-hexylthiophene) Crystalline Domains. *J. Phys. Chem. Lett.* **2014,** *5*, 399-403.

S4. Tamai, Y.; Ohkita, H.; Benten, H.; Ito, S. Exciton Diffusion in Conjugated Polymers: From Fundamental Understanding to Improvement in Photovoltaic Conversion Efficiency. *J. Phys. Chem. Lett.* **2015,** *6*, 3417-3428.

S5. Murata, Y.; Takeyama, T.; Sakamoto, Y.; Yamaguchi, K.; Tamai, Y.; Ohkita, H. Two-Dimensional Exciton Diffusion in an HJ-Aggregate of Naphthobisoxadiazole-Based Copolymer Films. *J. Phys. Chem. C* **2020,** *124*, 13063-13070.